



Contents lists available at ScienceDirect

# International Journal of Rock Mechanics and Mining Sciences

journal homepage: [www.elsevier.com/locate/ijrmms](http://www.elsevier.com/locate/ijrmms)

## Simulation of hydraulic fracturing processes in rocks by coupling the lattice Boltzmann model and the Park-Paulino-Roesler potential-based cohesive zone model

Luis A. Mejía Camones<sup>a</sup>, Eurípedes do A. Vargas Jr.<sup>a,\*</sup>, Raquel Q. Velloso<sup>a</sup>, Glaucio H. Paulino<sup>b</sup><sup>a</sup> Civil and Environmental Engineering Department, Pontifical Catholic University of Rio de Janeiro, Rua Marques de Sao Vicente 225, Rio de Janeiro, RJ 22453-900, Brazil<sup>b</sup> School of Civil and Environmental Engineering, Georgia Institute of Technology, 790 Atlantic Drive NW, Atlanta, GA 30332, USA

## ARTICLE INFO

## Keywords:

Crack propagation  
Hydraulic fracturing  
Lattice-Boltzmann model  
PPR cohesive-based zone model

## ABSTRACT

This paper contributes a scheme for two-dimensional (2D) numerical simulation of hydraulic fracturing processes in geological materials, which consists of a numerical coupling between the finite element method (FEM) and the lattice Boltzmann (LB) model. The Park-Paulino-Roesler potential-based cohesive zone model (PPR) is used to simulate the fracture propagation by means of interface finite elements, such that cohesive forces act on the fracture surface, capturing the softening process. The PPR model is used because it is a generalized fracture model that can represent the fracture process for mode I, mode II and mixed mode I-II, and can be applied to various materials, including heterogeneous materials, such as rock. The FEM and LB are coupled in an iterative process. The paper describes implementation details including procedures for coupling both methods. Examples of hydraulic fracturing process, modeled with the proposed FEM-LB coupling demonstrate the potential of this numerical procedure to model hydraulic fracturing processes in geomaterials of complex geometries.

## 1. Introduction

Numerical modeling of hydraulic fracturing has been performed using several methodologies, such as the finite element, extended finite element and discrete element methods. In general, fracture propagation in rocks has been evaluated for Mode I conditions. However, due to the complexity of the problem, few coupled fluid-mechanical techniques are available for the numerical modeling of hydraulic fracturing processes in media representing geological materials, in which Mode II or mixed (Modes I-II) ruptures also occur. In fact, geological media are discontinuous and heterogeneous materials, where fracture propagation may occur along paths with complex geometries, including deflections and bifurcations. Such geometric complexity hinders numerical modeling of hydraulic fracture propagation. In this context, the following factors must be considered in numerical models of hydraulic fracturing: (1) Development of a fracture model that can numerically simulate hydraulic fracturing in media similar to geological materials; (2) Development of a numerical model that simulates fluid flow inside a fracture independently of its shape.

Of the aforementioned factors, the fluid flow problem has been discussed less frequently in the technical literature. Numerous technical studies have focused on understanding the mechanical component of

the hydraulic fracturing process. However, the flow problem is still generally approached using lubrication theory, which is derived from the Navier-Stokes equations. Fluid flow through an irregular and complex fracture geometry, which can naturally develop in geological media, limits the use of the Navier-Stokes equations to determine the fluid macro-variables (e.g., the fluid velocity and pressure). Although lubrication theory may be a feasible approach to simulate the fluid flow problem, we focus on a different approach, as explained below.

An alternative approach to solve the fluid flow problem in hydraulic fracturing consists of using the lattice Boltzmann (LB) model, which has been used to model flow through porous media<sup>1</sup> and through irregular fractured media.<sup>2</sup> In both cases, the flow can be modeled numerically, independently of the fracture geometry, which is convenient to describe fracture in geological media. The LB model also allows fluid-structure interaction to be properly modeled, such as particles in suspension and/or their motion into the fluid due to drag forces. This feature of the LB model is particularly important when modeling hydraulic fracturing because, during crack propagation, the crack width may increase gradually with increasing injection pressure and its walls are considered to be a movable boundary condition.

The concept of cohesive fracture model has been used to model fracture in quasi-brittle materials.<sup>3–6</sup> Several cohesive fracture models

\* Corresponding author.

E-mail address: [vargas@puc-rio.br](mailto:vargas@puc-rio.br) (E.d.A. Vargas).<https://doi.org/10.1016/j.ijrmms.2018.09.003>

Received 8 January 2018; Received in revised form 12 September 2018; Accepted 29 September 2018

1365-1609/ © 2018 Elsevier Ltd. All rights reserved.

have been proposed to model the softening process during fracture; however, they have certain limitations. These limitations include artifacts in the numerical simulation of mixed-mode (Mode I-II) fracture propagation that consists of increasing tractions (positive stiffness) in the softening region.<sup>7</sup>

To circumvent the limitations of existing fracture models, Park *et al.*<sup>8</sup> introduced the Park-Paulino-Roesler (PPR) potential-based cohesive zone model. The PPR model is a general fracture model that describes macroscopic fracturing using interface elements, i.e. cohesive elements.<sup>7,8</sup> The PPR model can be used to simulate fracture of several types of materials and can be implemented in two ways: intrinsically (in which the interface elements are inserted into the finite element mesh at the beginning of the calculation) and extrinsically (in which the interface elements are inserted adaptively). This cohesive fracture model has been used to describe fracture propagation in quasi-brittle materials and materials with heterogeneous structures,<sup>9</sup> and it is ideal for describing fracture propagation in geomaterials.

The objective of this study is to develop a numerical procedure with fluid-mechanical coupling that can model the hydraulic fracturing process in geological materials while taking into account their heterogeneities and/or discontinuities. The LB model is used to describe single-phase fluid flow through complex fracture geometries. The finite element method (FEM) is implemented to model the mechanical component of crack propagation in an impermeable material. Communication between the two models will take place through the fracture walls or profiles, which are described by the PPR potential-based cohesive zone model. The extrinsic implementation of this fracture model will be utilized, in which the interface elements are inserted adaptively into the finite element mesh during crack growth.

## 2. Literature review

Numerical modeling techniques for hydraulic fracturing differ in their approaches to the mechanical process of crack propagation. Among several possibilities, these methodologies might be grouped in three approaches: based in the finite element method (FEM), based in the discrete element method (DEM), and based in the hybrid FEM-DEM method.

The FEM is commonly used to simulate numerically the propagation of a crack using either interface elements or extended finite elements. However, lubrication theory, which is derived from the Navier-Stokes equations, is typically used to model the flow of the pressurized fluid injected in the fracture. Lubrication theory is particularly useful to simulate fracture in homogeneous media, in which Mode I crack propagation occurs and the crack propagation path is known. In the extended finite element method (XFEM), a fracture can be modeled independently within a finite element mesh.<sup>10–14</sup> The fracture is represented virtually by enriching the nearby nodes using additional functions derived from the analytical solution to hydraulic fracturing in an elastic or poroelastic medium. The fact that the fracture does not depend on the finite element mesh increases the computational efficiency of this method. Nonetheless, this method has problems when the crack propagation path is irregular and may bifurcate or intercept other preexisting discontinuities. These problems may be minimized using interface elements. The use of this type of elements combined with lubrication theory to model the hydraulic fracturing has shown good results when compared to existing analytical solutions.<sup>15</sup>

Frydman and Fontoura<sup>16</sup> used interface elements in a finite element implementation to model hydraulic fracturing in a poroelastic material and achieved good results in comparison with laboratory test results. In their work, as also shown by Chen *et al.*,<sup>17</sup> it was observed that the necessary fluid pressure to create a hydraulic fracture is proportional to the material fracture energy. Modeling the fluid flow in the material during hydraulic fracturing allows one to investigate the influence of leak-off and material permeability on the injection fluid pressure, fracture length and width.<sup>18–21</sup> These hydraulic fracture characteristics

are also influenced by other factors, such as the material behavior and the confining stress. The width and length of a fracture have greater effects in a rigid material than in a ductile material,<sup>20</sup> and reductions in these fracture characteristics with increasing confining stress also have greater impact in rigid materials.<sup>15</sup> The fluid inside a propagating crack may not occupy its entire volume, and the fluid front may not coincide with the fracture front. Numerical modeling of this phenomenon and its effects was performed by Hunsweek *et al.*<sup>22</sup> using a fracture element that includes the effect of the difference between the fluid and fracture fronts and incorporating the relationship between the fracture propagation velocity and the fluid velocity. A fully coupled three-dimensional FEM was proposed by Salimzadeh *et al.*<sup>23</sup> to model hydraulic fracturing in permeable rocks. This model is used to investigate the applicability of the analytical solutions for penny shaped hydraulic fractures.

In addition to the FEM, the discrete element method (DEM) is an alternative method for numerically modeling the propagation of a hydraulic fracture with an irregular path, such as in a medium with discontinuities. In this method, the medium is composed of circular and polygonal particles (in the two-dimensional case) that interact through their contacts. The contacts have bonds that, when broken, represent the fracture. Torres and Castaño<sup>24</sup> showed the results of using the DEM to model the hydraulic fracturing process and observed path variations with different stress levels. These variations are also influenced by the presence of discontinuities.<sup>25</sup> The discrete element method has been coupled with the LB model to simulate sand production in oil wells,<sup>1</sup> in which the particle drag forces are calculated by the model. The same methodology has been used in hydraulic fracturing.<sup>26</sup> In this case, the fluid force that is calculated with the LB model is applied to the particles to initiate the fracture propagation. The limitation of the discrete element method in representing the mechanical behavior of a material is in determining the micro-parameters that represent its macroscopic behavior.<sup>27</sup> The calibration process for these parameters can be complex when the fracture parameters of the material are considered.

The hybrid FEM-DEM numerical technique that models fractures in rocky materials is a coupling between the finite element (FEM) and discrete element (DEM) methods.<sup>28–31</sup> In this case, interface elements are inserted between the elements of the finite element mesh before the beginning of the calculation (intrinsic approach). On these interface elements, a cohesive law is used to calculate the cohesive forces during the fracturing process. Once these elements have fractured, they can interact with one another through their contacts. This methodology can also be used in the numerical modeling of hydraulic fracturing, where the fluid pressure is calculated based on the change in the volume of the interface element.<sup>31</sup> Several authors use the cubic law to simulate the fluid flow into the interface elements in the coupling FEM-DEM and this methodology was successfully used to simulate the hydraulic fracturing including the effect of seepage. Additionally, the combination of the FEM-DEM with the cubic law can be complemented with the use of the Darcy's law to simulate the fluid flow into the rock matrix.<sup>32–36</sup>

The use of intrinsic interface elements avoids the need to constantly update element connectivities. Intrinsic interface elements are inserted into the mesh at the beginning of the calculation process, and require a high initial stiffness to model the pre fracture stage. The use of a high stiffness in these elements may increment the computational cost and create an artificial compliance with possible influence on the final results.<sup>9,37–39</sup> For that, the extrinsic approach, which is the technique adopted in the present study, is an attractive alternative because the interface elements are inserted adaptively into the finite element mesh to capture the fracturing process.

## 3. Numerical procedures for simulating hydraulic fracturing processes

In this study, the numerical modeling of hydraulic fracturing involves the interaction between two models. The first is a mechanical model that simulates the fracturing process, and the second is a flow

model that describes the injection of a fluid under pressure into a crack with a complex geometry and dimensions that may change depending on the volume of injected fluid. For the mechanical model, the aforementioned PPR cohesive zone model is implemented with extrinsic interface finite elements. These elements are used to simulate the crack propagation process. The finite element mesh describing the bulk material uses triangular elements with three nodes (T3), and the equilibrium equations are solved using the dynamic relaxation method.<sup>40</sup> The LB model was chosen to describe the fluid flow because of its ability to model the flow inside a fracture with an irregular geometry, even if its shape or dimensions vary continually.

### 3.1. PPR potential cohesive fracture model for fracture propagation in rocks

In continuum mechanics, the formulation of a linear elastic problem can be approached through the variational formulation. The finite elements method (FEM) discretizes the domain in elements where the variation of total potential energy in an element is minimized. Based in the principle of the virtual work, the variation of the total potential energy for each element implies that its value is zero.<sup>41</sup> Thus, applying this condition, the nodal internal forces of the element can be calculated from its stresses tensor. The solution of FEM using the dynamic relaxation solution (DR) involves the introduction of the equations of motion through the insertion of inertial nodal masses and viscous damping forces. The equations of motion<sup>42</sup> are:

$$\mathbf{M}\ddot{\mathbf{u}}' + \mathbf{C}\dot{\mathbf{u}}' + \mathbf{f}_{\text{int}}^e = \mathbf{f} \quad (1)$$

where  $\mathbf{M}$  is the mass matrix,  $\mathbf{C}$  is the damping matrix. The equation of motion may be solved by an explicit form through the central difference finite technique.<sup>43</sup> The resultant nodal force ( $\mathbf{FR}_i$ ) can be defined as:

$$\mathbf{FR}_i = \mathbf{f} - \mathbf{f}_{\text{int}}^e \quad (2)$$

where  $\mathbf{f}$  and  $\mathbf{f}_{\text{int}}^e$  forces corresponding to external and internal forces applied at node. If the  $\mathbf{FR}_i$  applied at node is a known, nodal displacements can be calculated using the Eq. (1). The DR can be defined as an iterative method where the unbalanced nodal forces into the FEM mesh generate nodal displacements that cause strains, stresses and internal forces (through a constitutive law) into the elements. These internal forces applied in the nodes generate new nodal displacements initiating an iterative process.

On the other hand, the PPR potential-based cohesive zone model<sup>7,8</sup> was proposed as a general model to describe a macroscopic physical fracture consistently with its boundary conditions. The PPR model has been implemented using both intrinsic and extrinsic cohesive elements. Due to the problems aforementioned, the intrinsic implementation is recommended for fractures with known paths.<sup>44</sup> This work uses the extrinsic implementation, in which the interface elements are inserted into the finite element mesh adaptively to capture the fracturing process. Fig. 1 shows the type of interface element that is used in this implementation. Each interface element has four nodes and it is inserted between bulk elements, which in our case are three-node triangular elements (T3). The purpose of the interface elements is to generate cohesive tractions that oppose the opening of the crack and relax the surrounding stresses in a region known as the cohesive fracture zone. The interface elements are inserted once the stress on a face shared by two elements of the finite element mesh reaches its tensile or shear strength. The insertion process is shown in Fig. 2. During this process, the normal (tensile) and tangential (shear) stresses that act on the mesh facets are constantly monitored (Fig. 2a). When the stresses on a facet exceeds the tensile or shear strength, an interface element is inserted at that location (Fig. 2b). Two interface elements that coincide at a node indicate that the node must be duplicated (Fig. 2c). After duplicating the node, with the generation of the fracture surface, the softening process is started (Fig. 2d). This type of implementation requires constant modifications to the topological information of the mesh due to the constant updating of the connectivity between the

elements. In the numerical implementation, the topological information is managed using the TopS library.<sup>45,46</sup>

In the extrinsic implementation of the PPR potential-based cohesive zone model, the fracture (which can be Mode I, Mode II or Mode I-II) is represented as follows. The fracturing process is initiated when the interface element is inserted into the FEM mesh. It occurs when the normal or tangential stress monitored on a facet achieve their strength limit values ( $\sigma_{\text{max}}$  or  $\tau_{\text{max}}$ ) respectively. The fracturing process is completed when the normal stress ( $T_n$ ) or the tangential stress ( $T_t$ ) on the cohesive element (which represents the cohesive fracture zone) vanishes. This occurs when the normal ( $\Delta_n$ ) or tangential ( $\Delta_t$ ) separation reach their maximum width ( $\delta_n$ ,  $\delta_t$ ). The area under the softening curve corresponds to the value of the fracture energy. The Mode I ( $\phi_n$ ) and Mode II ( $\phi_t$ ) fracture energies are:

$$\phi_n = \int_0^{\delta_n} T_n(\Delta_n, 0) d\Delta_n, \quad \phi_t = \int_0^{\delta_t} T_t(0, \Delta_t) d\Delta_t \quad (3)$$

Two shape parameters ( $\alpha$ ,  $\beta$ ) are introduced to characterize the softening of the material, which may behave as a brittle, plateau or quasi-brittle material (Figs. 3a and 3b).

The interface element used in the two-dimensional modeling in this study is shown in Fig. 3. The normal and tangential displacements ( $\Delta_n$ ,  $\Delta_t$ ) can be calculated from the nodal displacements measured in the local coordinate system “ $n - t$ ” ( $\tilde{u}$ ) (Fig. 3d), which are calculated from the displacements in the global coordinate system “ $X - Y$ ” ( $\tilde{u}$ ) (Fig. 3c). The potential function that describes the softening process (which determines the value of the normal stress ( $T_n$ ) or the tangential stress ( $T_t$ ) as a function of the normal and tangential widths ( $\Delta_n$ ) and ( $\Delta_t$ ), respectively) is:

$$\psi(\Delta_n, \Delta_t) = \min(\phi_n, \phi_t) + \left[ \Gamma_n \left( 1 - \frac{\Delta_n}{\delta_n} \right)^\alpha + (\phi_n - \phi_t) \right] \left[ \Gamma_t \left( 1 - \frac{|\Delta_t|}{\delta_t} \right)^\beta + \langle \phi_t - \phi_n \rangle \right] \quad (4)$$

where  $\Gamma_n$  and  $\Gamma_t$  are the energy constants, which are functions of the normal ( $\phi_n$ ) and tangential ( $\phi_t$ ) fracture energies, respectively, and  $\langle \cdot \rangle$  is the Macaulay bracket, which is evaluated as  $\langle x \rangle = (x + |x|)/2$ .

The normal and tangential stresses that act on the faces of the interface element vary according to its width, and their values can be calculated from the gradient of the potential function. Thus:

$$T_n(\Delta_n, \Delta_t) = \frac{\partial \psi(\Delta_n, \Delta_t)}{\partial \Delta_n} = -\alpha \frac{\Gamma_n}{\delta_n} \left( 1 - \frac{\Delta_n}{\delta_n} \right)^{\alpha-1} \left[ \Gamma_t \left( 1 - \frac{|\Delta_t|}{\delta_t} \right)^\beta + \langle \phi_t - \phi_n \rangle \right] \quad (5)$$

$$T_t(\Delta_n, \Delta_t) = \frac{\partial \psi(\Delta_n, \Delta_t)}{\partial \Delta_t} = -\beta \frac{\Gamma_t}{\delta_t} \left( 1 - \frac{|\Delta_t|}{\delta_t} \right)^{\beta-1} \left[ \Gamma_n \left( 1 - \frac{\Delta_n}{\delta_n} \right)^\alpha + \langle \phi_t - \phi_n \rangle \right] \frac{\Delta_t}{|\Delta_t|} \quad (6)$$

The stresses on the interface element generate cohesive tractions that act on the adjacent nodes. Thus, the tractions on this element decrease gradually with increases in the normal and tangential displacements of the faces of the interface elements. The final opening or displacement of the interface element faces defines the macroscopic fracture. Once the stresses have vanished, the fracture is considered open. The final opening values in the normal and tangential directions are  $\delta_n$  and  $\delta_t$ , respectively, and can be calculated from the fracture energy and the material cohesive strength:

$$\delta_n = \alpha \phi_n / \sigma_{\text{max}}, \quad \delta_t = \beta \phi_t / \tau_{\text{max}} \quad (7)$$

Once the stresses into the cohesive elements are calculated, their nodal internal forces can be calculated using the following equation:

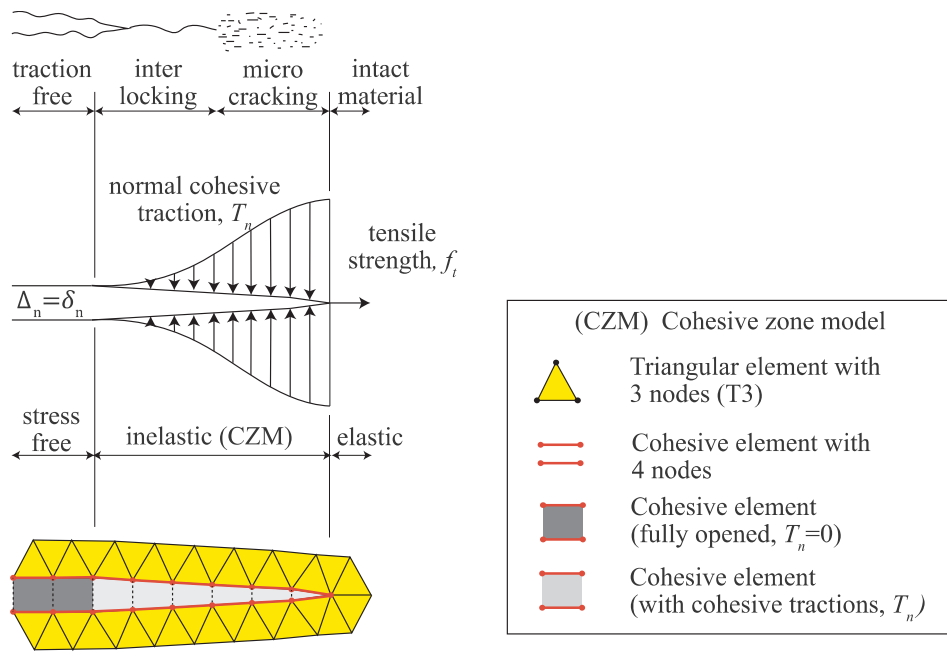


Fig. 1. Extrinsic implementation of the PPR potential-based cohesive zone model (adapted from Mahabadi<sup>67</sup>).

$$f_{coh} = \int_{\Gamma_c} [B_c]^T [T_c] dS \tag{8}$$

where,  $[B_c]$  is called the matrix that relates the global nodal displacements with the separation of the interface element faces and  $[T_c]$  is the

matrix of stresses.<sup>47</sup>

When the interface element is inserted into the FEM mesh to model the crack propagation process, the nodal internal forces calculated into the cohesive element should be applied to nodes of the adjacent bulk

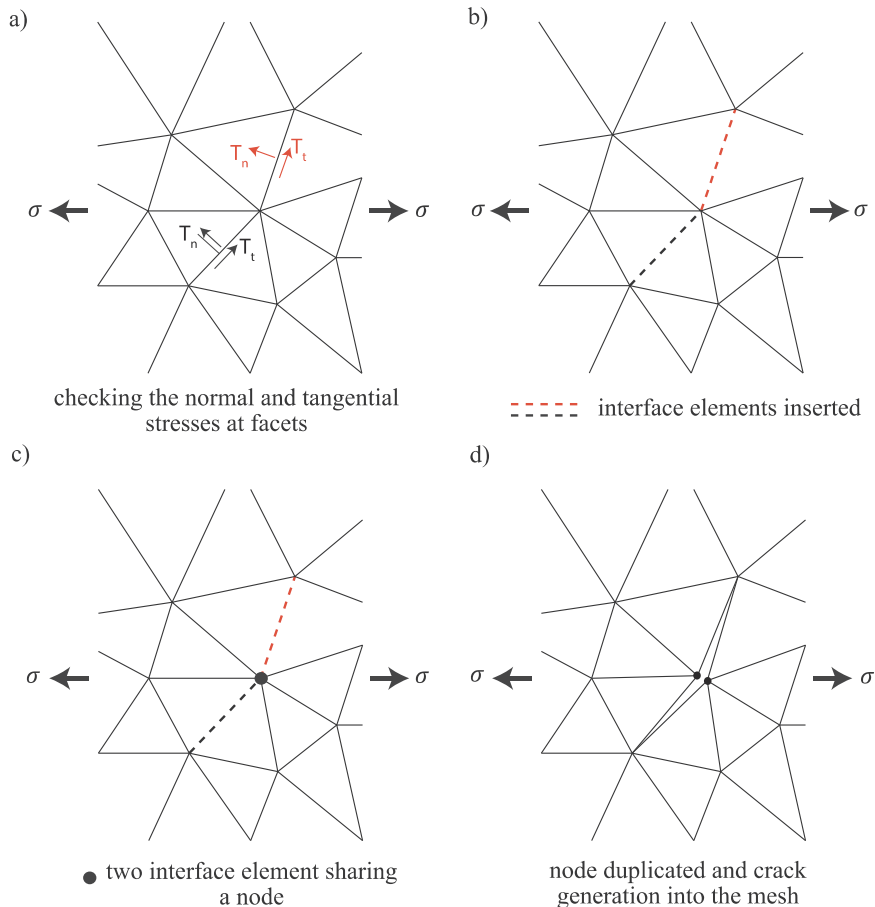


Fig. 2. Procedure of interface elements insertion in the extrinsic implementation and node duplication to create the fracture into the finite element mesh using the Tops data structure.

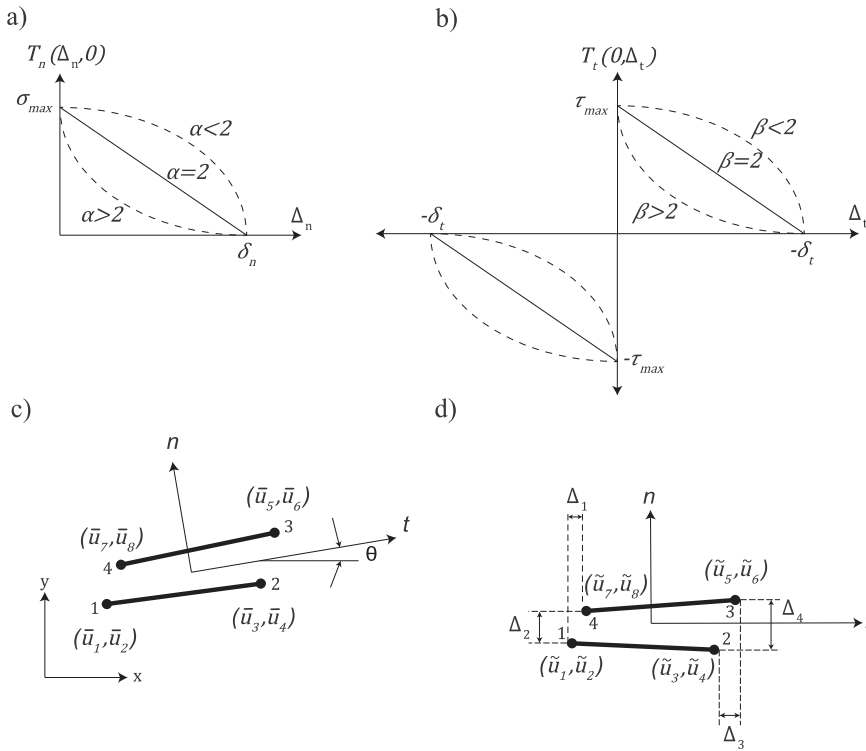


Fig. 3. a, b) Shape parameter ( $\alpha, \beta$ ) of the PPR potential-based cohesive zone model in the extrinsic cohesive zone model and the interface element used in the PPR potential-based cohesive zone model (adopted from Park and Paulino<sup>47</sup>), c) interface element in the global system coordinates “X-Y”; d) interface element in the local system coordinates “t-n”.

elements. Thus, the resultant forces in these nodes can be calculated adding the cohesive force from Eq. (8) in the Eq. (2):

$$\mathbf{FR}_i = \mathbf{f} - \mathbf{f}_{int}^e + \mathbf{f}_{coh} \quad (9)$$

### 3.2. The lattice Boltzmann (LB) method

At the macroscopic level, a fluid may be considered as a continuous medium in which the Navier-Stokes equations can be used to determine the macroscopic variables, such as the fluid velocity and pressure. These equations are difficult to solve due to their non-linearity but can be solved with numerical methods or analytically for several simple geometries.<sup>48</sup> If a fluid is approached from a discrete perspective, its motion may be determined through the interaction between the fluid particles. Newton's second Law can be used to determine the position of the particles for each time step, which are used to describe the flow at the macroscopic level. However, this calculation is unfeasible due to the large number of molecules that interact within a fluid (1 mol of water contains  $\sim 1023$  molecules). In order to overcome this issue, a third scale can be defined between the microscale and the macroscale, which is known as the mesoscale. At the mesoscale, the behavior of a set of particles is studied as a unit, whose properties are represented by a single function that is known as the distribution function.<sup>48</sup> In the lattice Boltzmann model, the particles are grouped according to their velocities and positions, and a distribution function  $f(\mathbf{x}, \mathbf{v}, t)$  used to define the probable number of particles at position  $\mathbf{x}$  at time  $t$  with velocity  $\mathbf{v}$ . Because there are no interactions between the particles, and the number of particles is conserved when they move from position  $\mathbf{x}$  to position  $\mathbf{x} + \mathbf{v}dt$ , we have:

$$f\left(\mathbf{x} + \mathbf{v}dt, \mathbf{v} + \frac{\mathbf{F}}{m}dt, t + dt\right) dx d\mathbf{v} - f(\mathbf{x}, \mathbf{v}, t) dx d\mathbf{v} = 0 \quad (10)$$

However, collisions between particles may add or remove some from the volume element  $dx dy$ . The variation between the final and initial distribution functions is known as the collision operator,  $\delta_c$ , which is defined by:

$$\begin{aligned} f\left(\mathbf{x} + \mathbf{v}dt, \mathbf{v} + \frac{\mathbf{F}}{m}dt, t + dt\right) dx d\mathbf{v} - f(\mathbf{x}, \mathbf{v}, t) dx d\mathbf{v} \\ = \delta_c(\mathbf{x}, \mathbf{v}, t) dx d\mathbf{v} dt \end{aligned} \quad (11)$$

Considering that  $f$  is a function of  $\mathbf{x}$ ,  $\mathbf{v}$  and  $t$ , Eq. (11) can be rewritten as:

$$\frac{\partial f}{\partial t} + \frac{\partial f}{\partial \mathbf{x}} \cdot \mathbf{v} + \frac{\mathbf{F}}{m} \cdot \frac{\partial f}{\partial \mathbf{v}} = \delta_c \quad (12)$$

Eq. (12) represents the Boltzmann equation, and the collision term must be consistent with the mass and momentum conservation laws. The collision term transforms the Boltzmann equation into a nonlinear integro-differential form<sup>49</sup> to become an implicit equation that can be linearized and turned explicit through the so-called Bhatnagar-Gross-Krook (BGK) approximation.<sup>50,51</sup>

#### 3.2.1. The BGK approximation

A commonly used version of the collision term is the BGK approximation,<sup>50,52</sup> which is calculated as follows:

$$\delta_c = \frac{1}{\tau} (f^{eq}(\mathbf{x}, \mathbf{v}, t) - f(\mathbf{x}, \mathbf{v}, t)) \quad (13)$$

where  $\tau$  is the collision term, and  $f^{eq}$  is defined as the equilibrium function. To simplify the BGK approximation process, the space is discretized so that the particles can only reside at the lattice nodes and can move in fixed directions during defined time intervals (space discretization). For the two-dimensional case, the **D2Q9** (two dimensions, nine velocity directions) lattice model is used (Fig. 4a) with fixed velocities  $\mathbf{v}_\alpha$  that can be expressed as follows<sup>53</sup>:

$$\mathbf{v}_\alpha = \begin{cases} (0, 0) & \alpha = 0 \\ \left( \cos\left[\frac{(\alpha-1)\pi}{2}\right], \sin\left[\frac{(\alpha-1)\pi}{2}\right] \right) c & \alpha = 1, 2, 3, 4 \\ \left( \cos\left[\frac{(\alpha-5)\pi}{2} + \frac{\pi}{4}\right], \sin\left[\frac{(\alpha-5)\pi}{2} + \frac{\pi}{4}\right] \right) \sqrt{c} & \alpha = 5, 6, 7, 8 \end{cases} \quad (14)$$

where  $c = \Delta x / \Delta t$ , in which  $\Delta x$  and  $\Delta t$  correspond to the cell size and the established time step, respectively. Constraining the velocity to

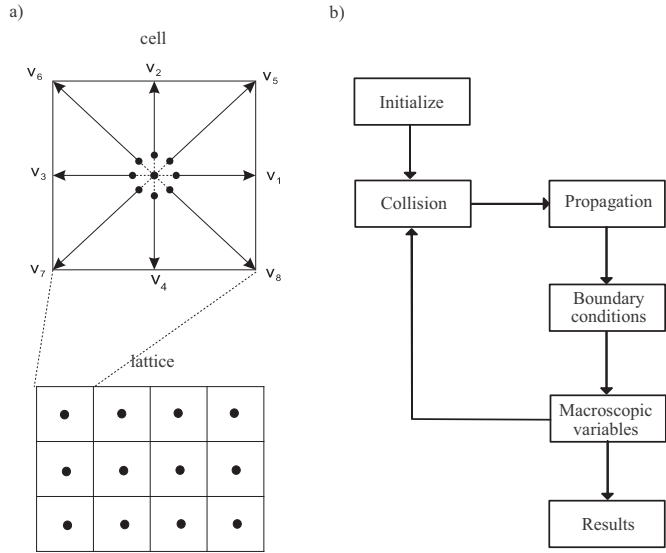


Fig. 4. a) D2Q9 lattice Boltzmann cell (Two dimension, nine velocities); b) illustration of the calculation process of lattice Boltzmann model.

certain directions, and discretizing time, allow one to rewrite Eq. (11) as shown:

$$f_{\alpha}(\mathbf{x} + \mathbf{v}_{\alpha}\Delta t, t + \Delta t) - f_{\alpha}(\mathbf{x}, t) = \frac{\Delta t}{\tau} \left[ f_{\alpha}^{eq}(\mathbf{x}, t) - f_{\alpha}(\mathbf{x}, t) \right] \quad (15)$$

where  $\tau$  is the collision time (which is a function of the fluid viscosity), and  $f^{eq}$  is the equilibrium function. This function, which is derived from the Maxwell distribution function,<sup>54</sup> depends on macroscopic variables, such as velocity  $\mathbf{u}$  and density  $\rho$  of the fluid. The equilibrium function for the case of the D2Q9 cell is defined as:

$$f_{\alpha}^{eq}(\mathbf{x}, t) = \omega_{\alpha} \rho \left[ 1 + 3 \frac{(\mathbf{v}_{\alpha} \cdot \mathbf{u})}{c^2} + \frac{9}{2} \frac{(\mathbf{v}_{\alpha} \cdot \mathbf{u})^2}{c^4} - \frac{3}{2} \frac{\mathbf{u} \cdot \mathbf{u}}{c^2} \right] \quad (16)$$

where  $\omega_{\alpha}$  are constants defined as:

$$\omega_{\alpha} = \begin{cases} 4/9 & \alpha = 0 \\ 1/9 & \alpha = 1, 2, 3, 4 \\ 1/36 & \alpha = 5, 6, 7, 8 \end{cases} \quad (17)$$

For each time step  $\Delta t$ , the fluid macroscopic variables (i.e., fluid velocity and density) can be calculated from the distribution function (Eq. (15)) as follows:

$$\rho(\mathbf{x}, t) = m \sum_{\alpha=1}^b f_{\alpha}(\mathbf{x}, t) \quad , \quad \mathbf{u}(\mathbf{x}, t) = \frac{m}{\rho(\mathbf{x}, t)} \sum_{\alpha=1}^b \mathbf{v}_{\alpha} f_{\alpha}(\mathbf{x}, t) \quad (18)$$

Two conditions must be taken into account to determine the fluid macroscopic behavior, which therefore correspond to the Navier-Stokes equations: a) in an incompressible fluid, the density is equal to an approximately constant value, with  $\Delta\rho/\rho \ll 1$ ; and b) the Mach number is defined as  $Ma = u_{max}/c_s \ll 1$ . The variable  $u_{max}$  corresponds to the maximum flow velocity, and  $c_s$  is the pseudo-velocity of sound in the fluid, which is defined as  $\sqrt{c^2/3}$ . The BGK approximation allows the Navier-Stokes equations for a compressible fluid to be solved at the incompressibility limit.<sup>55</sup> Any deviation from either of these conditions may lead to an error, which is known as the compressibility error.<sup>56</sup> The fluid pressure  $p$  can be calculated as a density function using the general gas equation,<sup>52</sup>  $p = \rho c_s^2$ . These considerations indicate that the only way to impose a pressure gradient to generate a flow is by imposing a density gradient because the pressure is not an independent variable. Calculation errors may occur if the pressure gradient is large. He and Luo<sup>53</sup> proposed an approach for this type of problems by introducing a local pressure distribution function that is defined as  $p_{\alpha} = c_s^2 f_{\alpha}$ , where

the equilibrium function in terms of pressure is defined by:

$$p_{\alpha}^{eq}(\mathbf{x}, t) = \omega_{\alpha} \left\{ p + p_0 \left[ 3 \frac{(\mathbf{v}_{\alpha} \cdot \mathbf{u})}{c^2} + \frac{9}{2} \frac{(\mathbf{v}_{\alpha} \cdot \mathbf{u})^2}{c^4} - \frac{3}{2} \frac{\mathbf{u} \cdot \mathbf{u}}{c^2} \right] \right\} \quad (19)$$

Thus, the LB evolution equation for an incompressible fluid is obtained as:

$$p_{\alpha}(\mathbf{x} + \mathbf{v}_{\alpha}\Delta t, t + \Delta t) = p_{\alpha}(\mathbf{x}, t) - \frac{1}{\tau^*} [p_{\alpha}(\mathbf{x}, t) - p_{\alpha}^{eq}(\mathbf{x}, t)] \quad (20)$$

where  $\tau^*$  is the dimensionless collision time, which is defined as  $\tau^* = \tau/\Delta t$ . Analogous to Eq. (18), the macroscopic variables can be calculated as:

$$p(\mathbf{x}, t) = m \sum_{\alpha=1}^b p_{\alpha}(\mathbf{x}, t) \quad , \quad p_0 \mathbf{u}(\mathbf{x}, t) = \sum_{\alpha=1}^b \mathbf{v}_{\alpha} p_{\alpha}(\mathbf{x}, t) \quad (21)$$

Generally, the solutions to the lattice-Boltzmann model equations are obtained in two stages, collision and propagation, whose equations are derived from Eq. (20) and are defined by:

$$p'_{\alpha}(\mathbf{x}, t) = p_{\alpha}(\mathbf{x}, t) - \frac{1}{\tau^*} [p_{\alpha}(\mathbf{x}, t) - p_{\alpha}^{eq}(\mathbf{x}, t)],$$

$$p_{\alpha}(\mathbf{x} + \mathbf{v}_{\alpha}\Delta t, t + \Delta t) = p'_{\alpha}(\mathbf{x}, t) \quad (22)$$

Fig. 4b shows the calculation process of the lattice Boltzmann model, including the two stages. The pressure distribution function is calculated at each time step. The boundary conditions are then imposed, and the fluid's macroscopic variables are calculated. When compared with the conventional formulation, this type of approach allows larger pressure gradients to be adopted.

### 3.2.2. Boundary conditions

The boundary conditions in the lattice Boltzmann model, which are controlled by the solids in the model, can be fixed or mobile. Because one of the objectives of this study is to evaluate hydraulic fracturing, the propagating fracture imposes a mobile boundary condition. In general, the cells are identified as representing a solid or a liquid with the numbers 1 and 0, respectively. Noble and Torczynski<sup>57</sup> proposed a solution for boundaries in which a cell that is located at the solid-liquid interface will have a value between 0 and 1 that corresponds to its solid fraction. Thus, the lattice-Boltzmann equation becomes:

$$p_{\alpha}(\mathbf{x} + \mathbf{v}_{\alpha}\Delta t, t + \Delta t) = p_{\alpha}(\mathbf{x}, t) - \frac{1}{\tau^*} (1-B) [p_{\alpha}(\mathbf{x}, t) - p_{\alpha}^{eq}(\mathbf{x}, t)] + B \Omega_{\alpha}^s \quad (23)$$

where  $B$  is the weight function, which is given by:

$$B(\mathbf{x}, t) = \frac{\epsilon(\mathbf{x}, t)(\tau^* - 0.5)}{1 - \epsilon(\mathbf{x}, t) + (\tau^* - 0.5)} \quad (24)$$

where  $\epsilon$  is the solid fraction, and  $\Omega_{\alpha}^s$  is an additional collision term that modifies the pressure distribution functions to treat obstacles based on the bounce-back concept that is given by:

$$\Omega_{\alpha}^s = p_{-\alpha}(\mathbf{x}, t) - p_{\alpha} + p_{\alpha}^{eq}(p, \mathbf{v}_p) - p_{-\alpha}^{eq}(\mathbf{x}, t) \quad (25)$$

where  $\mathbf{v}_p$  is the velocity of the solid at position  $\mathbf{x}$  and time  $t$ , and  $-\alpha$  represents the direction opposite to the  $\alpha$  direction. This model has successfully been used in fluid-mechanical coupling with the discrete element method<sup>1</sup> to model flow through porous media. Fig. 5a and Fig. 5b show the boundary definition using the solid fraction compared to the traditional method.

## 4. A coupled PPR-LB framework for hydraulic fracturing

The PPR potential-based cohesive zone model is used to simulate the crack propagation during hydraulic fracturing. The fracture geometry, which is obtained from the inserted interface elements, is used to generate the Boltzmann lattice and thus defines the cells that

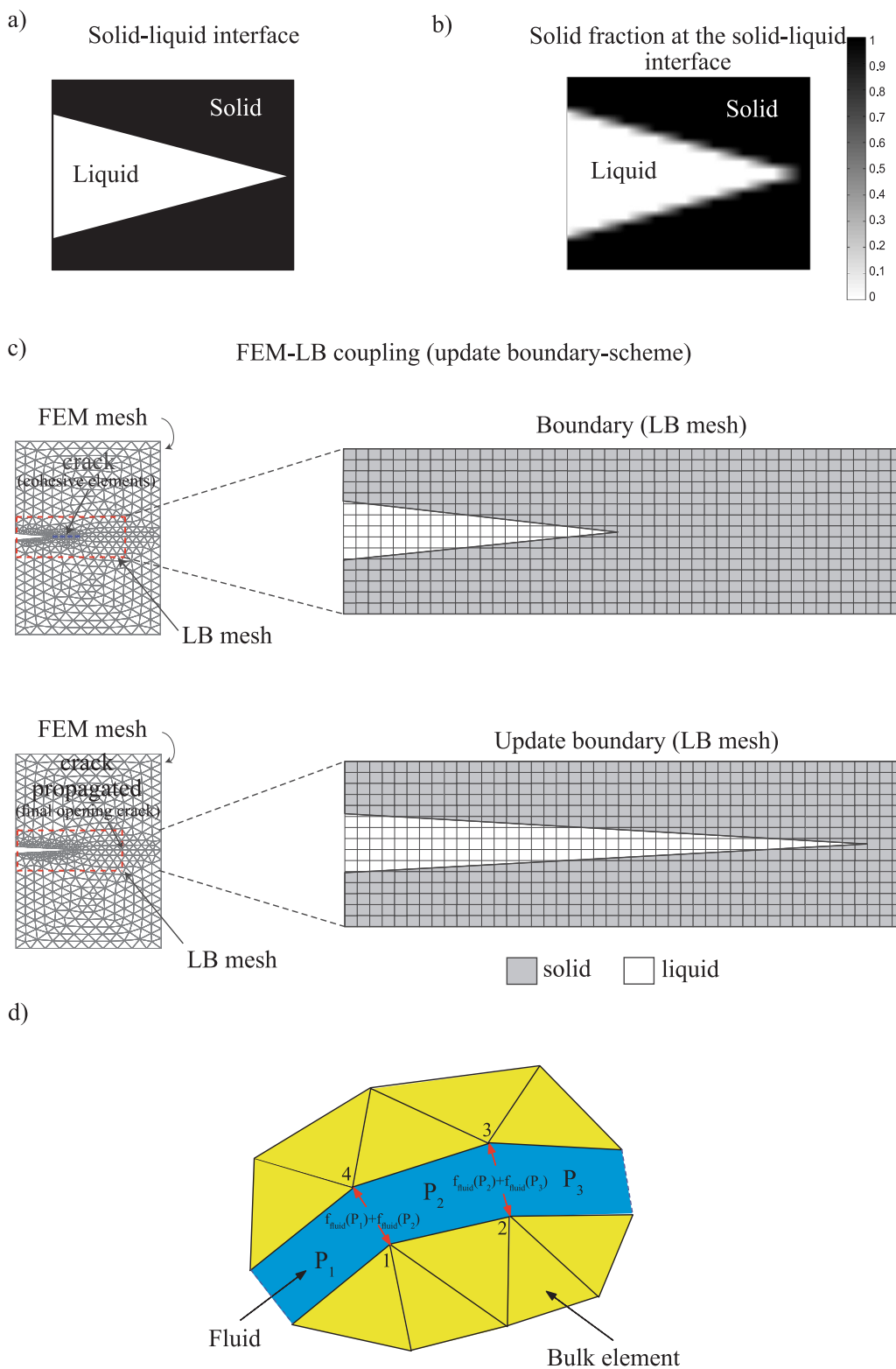


Fig. 5. a,b) Examples of the liquid-solid boundary in LB model using the fraction solid method; c) detail of the two meshes used in the FEM-LB coupling process. The LB mesh is created in the zone where the fracture propagation happens; and d) scheme of fluid force transfer to FEM from LB,  $f_{fluid}(P_1)$  and  $f_{fluid}(P_2)$  are the fluid force due to the fluid pressure  $P_1$  and  $P_2$  respectively.

correspond to the solids, liquids and solid-liquid interfaces. The number of cells in the interface element ( $N$ ) is defined using their normal final opening ( $\delta_n$ ) and an appropriate the Knudsen number ( $K_n$ ) value to ensure a continuum fluid (normally  $K_n \leq 0.001$ ).<sup>58</sup> Two superimposed meshes are used to couple these two methodologies (Fig. 5c). The first

mesh corresponds to the finite element mesh that is used to model the fracture propagation in an impermeable material, and the second mesh, which corresponds to the Boltzmann lattice, is used to impose the single-phase fluid pressure condition inside the fracture to cause its propagation. The Boltzmann lattice is fixed in the region where the

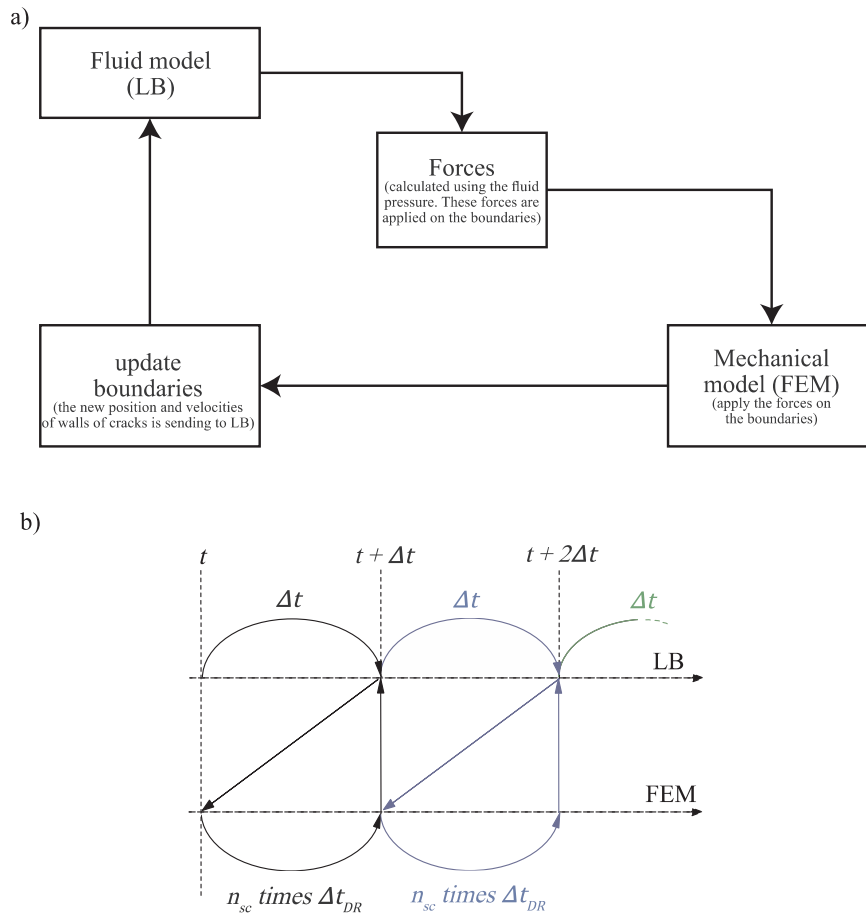


Fig. 6. a) Scheme of the calculation process between FEM and LB model for each sub-cycle in the coupling procedure; b) relation between the timesteps of LB and FEM models. One interaction of the LB needs  $n_{sc}$  interactions of the FEM model.

fracture propagation is expected to occur. To illustrate, Fig. 5d shows the scheme to transfer the fluid force to FEM. The calculation process is showed in Fig. 6a. The fluid pressure, which is calculated by the LB model, is used to calculate the force with which the fluid acts on the fracture walls ( $f_{fluid}$ ). For example, in Fig. 5d, the  $f_{fluid}$  applied on node 1 is equal to  $f_{fluid}(P_1) + f_{fluid}(P_2)$ , where  $P_1$  and  $P_2$  are the fluid pressure into the interface elements that share the node 1. This force  $f_{fluid}$  is transferred to the finite elements, where it is applied to the nodes of the fracture walls as an external force. Thus, Eq. (9) used to calculate the resultant nodal force in these nodes must include the fluid forces:

$$FR_i = f - f_{int}^e + f_{coh} + f_{fluid} \quad (26)$$

The application of this resultant force causes the walls to move, which modifies the crack width. The new positions of these walls and their displacement velocities, which are calculated in the FEM, are transferred to the LB model, where the solid-liquid boundaries are updated, and the process resumes recalculating the fluid pressure inside the crack. It is important to note that the coupling between FEM (mechanical model) and LB (fluid model) is done in two ways. Thus, changes in the fluid domain due to fracture growth have influence in the calculation of the fluid macro variables. From a mechanical point of view, the force generated by the fluid pressure acts as an external force applied onto the fracture walls, modifying the fracture shape. This fracture deformation changes the fluid domain, which means that LB considers in its calculation process the influence of the fracture shape modification. For that, in each *timestep*, the position of the fracture boundary is updated and its velocity is introduced into the calculation process (Eq. (25)).

The computational implementation contains two modules for each

part of the problem. The mechanical module that simulates the strains and the fracturing process of the material, and the fluid module that simulates the flow of a pressurized fluid injected into a fracture. Each of these modules has its own timestep. The coupling of these two methodologies involves the use of two time steps. Normally, the FEM time step ( $\Delta t_{DR}$ ) is smaller than the LB time step ( $\Delta t$ ). A new parameter, the sub-cycle ( $n_{sc}$ ), is defined as:

$$n_{sc} = \Delta t / \Delta t_{DR} \quad (27)$$

Thus,  $n_{sc}$  FEM time steps are necessary for every LB time step. Fig. 6b shows the numerical models interaction and the relation between their timesteps during the calculation process.

### 5. Results

This section presents modeling of hydraulic fracturing processes using the simulation scheme presented in this work. We make comparison between the numerical results and the analytical solution for hydraulic fracturing in Mode I for homogeneous media. The results of the crack propagation in heterogeneous media will be discussed, and finally, a comparison is presented between the results obtained using the developed numerical procedures and those from an experiment concerning the determination of trajectories of crack propagation in Modes I-II of hydraulic fracturing in a granite sample. The number of cells into the interface element was calculated using the Knudsen number ( $K_n = \nu_{LB} / (c_s N)$ ),<sup>59</sup> where  $\nu_{LB}$  denotes kinematic viscosity in lattice-Boltzmann units. For the first example four cells ( $N = 4$ ) were considered. This value corresponds to a  $K_n$  value slightly close to 0.001, but it is sufficient to ensure a continuum fluid. It should be noted that

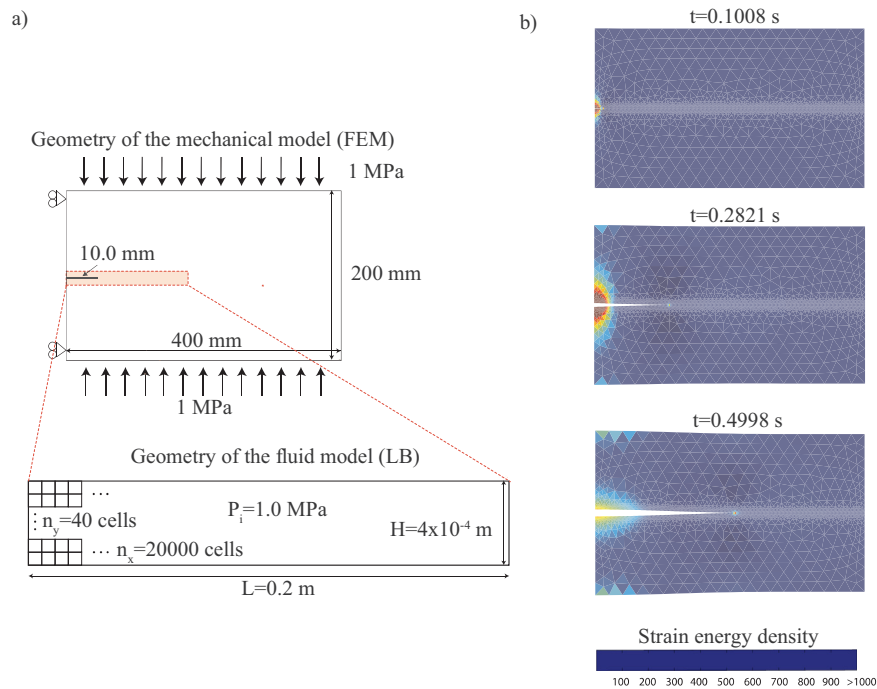


Fig. 7. a) Geometry and modeling boundary conditions of hydraulic fracturing process through FEM-LB numerical coupling. The fluid mesh model is located at the sample center (in red) to capture the fracture propagation; b) fracture propagation due to the injection of pressurized fluid.

the value of  $N$  is an initial value. The number of cells is a variable number that increases during the fluid injection due the crack opening. In the other examples, the value of  $\Delta x$  is increased in order to reduce the computational effort assuming that  $K_n$  may achieve an appropriate value during the process of crack opening.

### 5.1. Verification of numerical implementation with analytical solutions for Mode I fracture

To compare the results of the numerical solution to the analytical solutions for the hydraulic fracturing process, a hypothetical model was created that considers a toughness regime. This regime assumes that the energy necessary to create the fracture is greater than the energy dissipated by the viscous fluid,<sup>60</sup> which means that this solution is independent of the fluid viscosity. The model geometry and boundary conditions and results are shown in Fig. 7a. The Young's modulus and Poisson ratio of the material are  $E = 5.0$  GPa and  $\nu = 0.2$  respectively. The fracture properties used for the cohesive elements are:  $\sigma_n = \sigma_t = 1$  MPa,  $\phi_n = \phi_t = 20$  N/m and  $\alpha = \beta = 2$ . The parameters used in the LB model are: flow ratio  $Q = 7.6 \times 10^{-5}$  m<sup>3</sup>/s,  $\Delta x = 10^{-5}$  m,  $\Delta t = 1.5 \times 10^{-6}$  s, fluid density  $\rho = 1000$  kg/m<sup>3</sup> and kinematic viscosity  $\nu = 1.5 \times 10^{-6}$  m<sup>2</sup>/s. Because the goal is for the fracture to propagate as a Mode I rupture, its path is predictable, and thus a large LB mesh is not needed. This comparison is useful for understanding how this coupling technique approaches the analytical results, even when considering different working hypotheses.

The first hypothesis is related to the mechanical process. The numerical model (FEM) considers that the fracture is opened once the cohesive process is finished. This cohesive process (which occurs in the fracture tip) is a non-linear problem not considered by the analytical formulations based in the linear elastic fracture mechanics. The analytical models KGD and PKN admit that the cohesive zone is negligible. Thus, for the analytical evaluation, the fracture is considered opened when the stress achieves its maximum value. The second hypothesis is related to the fluid process modeling. The numerical model (LB) simulates the fluid flow in a continuum media through the flow of particles in a discretized media. In order to simulate the flow through

parallel plates(hypothesis considered in the analytical models<sup>61</sup>), LB requires an adequate number of cells (defined by Knudsen number) inside the fracture and certain number of calculation cycles to reproduce the Poiseuille profile of the velocity.<sup>62</sup> The LB precision can be improved increasing the number of cells into the fracture, but it raises the computational cost. It is important to note that this verification work is not intended to reproduce the KGD and PKN models.

Figs. 7b and 8 show the results for the fluid injection pressure and the fracture width and length, respectively. Fig. 7b shows the strain energy density during the crack growth due to the fluid injection. It is observed that strain energy density decreases when the crack propagation occur. The decrease of the strain energy density corresponds to the decrease of the injected fluid pressure that happens after the rock fracture pressure is reached. The curves for the injection pressure differ because the coupled FEM-LB method is able to model the complete injection process, beginning with the fracture pressure and the propagation pressure (Fig. 8a), which is not possible with the analytical solution. That is because the analytical formulation only models the injection fluid pressure during fracture propagation until it reaches the propagation pressure.

The numerical results show that, before reaching the peak injection fluid pressure, several interface (cohesive) elements are inserted into the mesh to begin the fracturing process. From that point on, the fluid injection pressure increases until reaching a maximum value (fracture pressure). After this peak, the fluid injection pressure obtained from the analytical solution and the numerical solution are similar, although there are some path differences. The fluid injection pressure decreases more quickly in the analytical solution than in the numerical solution and reaches a higher propagation pressure.

However, even with these differences, both solutions are acceptable because their fracture propagation paths are similar. Both solutions provide acceptable results for the fracture width (Fig. 8b) and length (Fig. 8c).

### 5.2. Hydraulic fracturing in fractured medium

In a geological medium, the propagation of a fracture due to

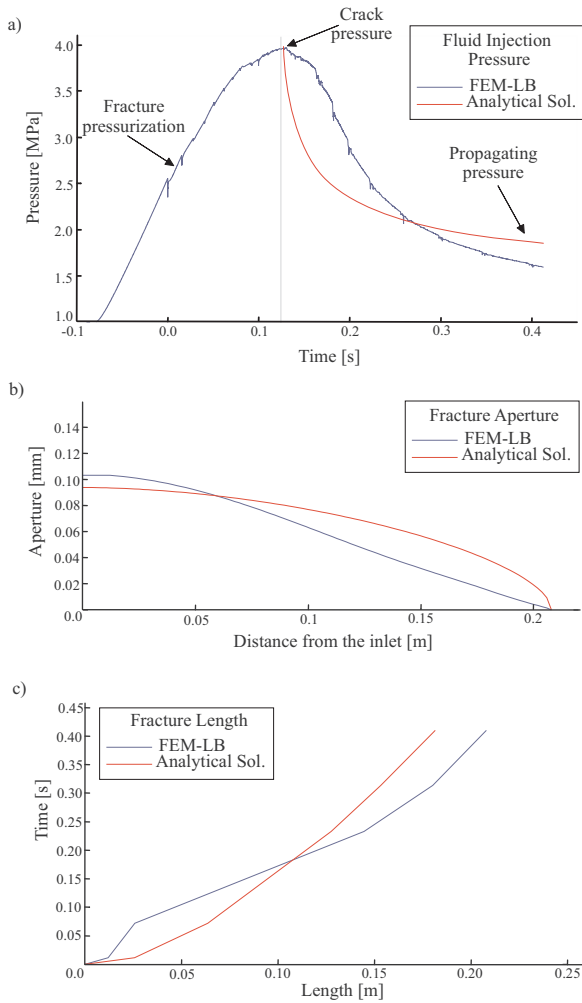


Fig. 8. Comparison between the results obtained through FEM-LB coupling and the analytical solution. a) values of pressurized fluid injected into the fracture in the toughness regime; b) values of fracture aperture and c) values of fracture length.

injection of a pressurized fluid can intercept preexisting fractures. Experimental and numerical works show that, depending on the

preexisting discontinuity aperture or shear strength properties, a hydraulic fracture can either cross or bypass it.<sup>63,64</sup> In order to analyze the influence of preexisting discontinuities in the hydraulic fracture propagation path, two cases are analyzed considering the geometry and boundary conditions in Fig. 9a. In case 1, the discontinuity has fracture strength properties equal to 10% of the strength properties of the surrounding rock; and in case 2, the discontinuity strength properties are equal to 50% of those of the surrounding rocks. The Young's modulus and Poisson ratio of the material are  $E = 5.0 \text{ GPa}$  and  $\nu = 0.2$  respectively. The fracture properties used for the cohesive elements are:  $\sigma_n = \sigma_t = 1 \text{ MPa}$ ,  $\phi_n = \phi_t = 10 \text{ N/m}$  and  $\alpha = \beta = 2$ . The parameters adopted in the LB model are: flow ratio  $Q = 1.7 \times 10^{-4} \text{ m}^3/\text{s}$ ,  $\Delta x = 5.0 \times 10^{-5} \text{ m}$ ,  $\Delta t = 5.0 \times 10^{-6} \text{ s}$ , fluid density  $\rho = 1000 \text{ kg/m}^3$  and kinematic viscosity  $\nu = 2.0 \times 10^{-6} \text{ m}^2/\text{s}$ .

The mechanical properties of existing fractures may influence the trajectory of a hydraulically driven fracture. When a hydraulic fracture approaches an existing fracture, two regions of analysis can be defined. The first corresponds to the region between the propagating fracture and the nearest wall of the existing fracture. The second corresponds to the region containing the remaining wall as can be seen in Fig. 9b–c. A continuous injection of fluid under pressure in the hydraulic fracture tends to increase its opening, thus having the effect of producing shear stresses in the preexisting fracture as depicted in Figs. 9b and 9c. If the shear strength of the preexisting fracture is high, tensile stresses may be generated in the wall located ahead of the hydraulic fracture. In this case, considering that the tensile stresses exceed the tensile strength of the rock, the hydraulic fracture will not change its path and will cross the preexisting fracture (Fig. 9c).

On the other hand, if the shear strength of the existing fracture is low, the walls of the preexisting fracture may experience relative movement, facilitating the propagation of the existing fracture as shown in Fig. 9b. In this case, the hydraulic fracture propagation may change direction, initially following the existing fracture.

The numerical results for this case, using the procedures described in the present paper, are shown in Fig. 10a. It shows the fracture propagation evolution and the fluid front associated to both cases described above. In case 1, after the connection between the propagating fracture and the preexisting discontinuity, the fracture propagation path is deviated by the discontinuity and the fracture continues to propagate from its ends. In case 2, the discontinuity has a higher shear strength and the fracture propagation crosses the preexisting discontinuity. The FEM meshes containing the hydraulic fracture are shown in Fig. 10b for both cases studied. Three refined mesh levels

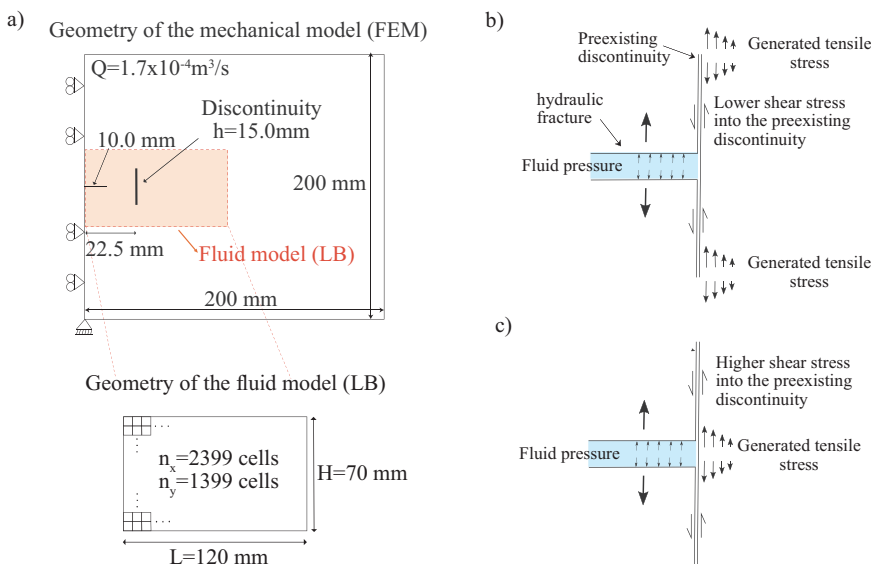


Fig. 9. a) Geometry and modeling boundary conditions of the hydraulic fracturing process in a fractured medium. Hydraulic fracture in a medium with discontinuity, b) hydraulic fracture intercepts a preexisting discontinuity creating low shear stress which produces tensile stresses at the preexisting discontinuity tips; c) hydraulic fracture intercepts a preexisting discontinuity creating high shear stress inside it, which produces tensile stress at its front.

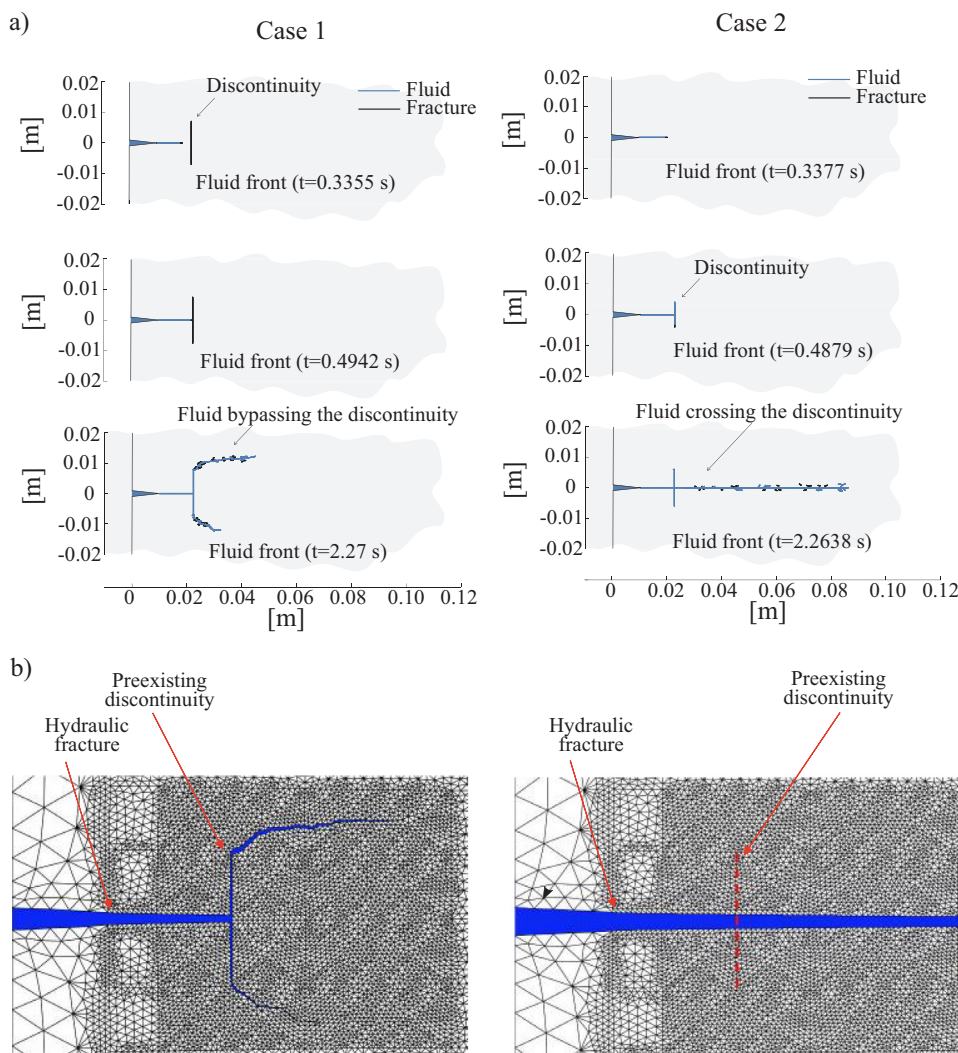


Fig. 10. a) Fracture growth in a fractured medium. The black lines show the interface elements inserted into the finite element mesh. The blue lines show the interface elements containing the injected fluid. In case 1, fracture propagation path bypass the preexisting discontinuity. In case 2, the fracture propagation path cross it; b) Finite element mesh showing the hydraulic fracture propagation into a discontinuous medium. The left picture shows the hydraulic fracture bypassing a preexisting discontinuity and the right picture shows the hydraulic fracture crossing a preexisting discontinuity. The blue line represents the fluid injected into the fracture.

have been used in the numerical simulation. Coarse mesh was used in a region containing the initial crack where the fluid is injected. Finer mesh was used between the initial crack tip and the area close to the preexisting discontinuity; and an even finer mesh was used in the area where the hydraulic fracture may propagate. The mesh in this area must be refined in order to capture the hydraulic fracture path accurately.

The obtained results are similar in qualitative terms to the ones obtained by Blanton<sup>65</sup> who conducted an experimental investigation. The experiments showed that for a higher normal stress applied normal to the preexisting fracture, the hydraulic fracture tends to cross it. This is equivalent to having a higher shear strength as presented above.

### 5.3. Hydraulic fracturing in heterogeneous media

As discussed previously, one of the characteristics of geological materials is their heterogeneity. Because rock is considered to be an aggregate that is composed of one or more minerals or clasts with different mechanical properties, the propagation of a fracture in this medium results in a tortuous path that is difficult to model analytically or numerically using conventional FEM. For this reason, the coupled FEM-LB method is proposed to model a hydraulic fracturing process that is as similar as possible to the physical phenomenon. To evaluate the simulation of this process in a heterogeneous material, a hypothetical model was developed for a medium with rigid inclusions of another material, which are placed in front of the initial fracture in which the fluid will be injected. Fig. 11a shows the inclusions, the geometry,

and the boundary conditions of the problem. The Young's modulus and Poisson ratio of the material are  $E = 5.0$  GPa and  $\nu = 0.2$  respectively. The fracture properties used for the cohesive elements are:  $\sigma_n = \sigma_t = 1$  MPa,  $\phi_n = \phi_t = 10$  N/m and  $\alpha = \beta = 2$ . The parameters used in the LB model are: flow ratio  $Q = 1.7 \times 10^{-4}$  m<sup>3</sup>/s,  $\Delta x = 5.0 \times 10^{-5}$  m,  $\Delta t = 5.0 \times 10^{-6}$  s, fluid density  $\rho = 1000$  kg/m<sup>3</sup> and kinematic viscosity  $\nu = 2.0e^{-6}$  m<sup>2</sup>/s. The stiffness and fracture strength of the rigid inclusions were 10 times higher than those of the matrix. However, the contacts between these inclusions and the matrix represent a heterogeneity and their fracture strength is 10% of that of the matrix.

Figs. 11b and 12 show the results of the simulation. Fig. 11b shows that the fracture circumvents the rigid inclusions without breaking them. This occurs because the contacts between the inclusions and the matrix had low fracture resistance. Because the fluid injection modifies the stress field at the tip of the crack, the contacts between the rigid inclusions and the matrix rapidly fractures, and it is necessary to insert interface (cohesive) elements in these locations. For the fluid to enter the fracture, it is necessary for the interface element that is inserted into the finite element mesh to be in contact with another interface element that contains fluid and therefore applies pressure on its walls to open the fracture. This is shown in Fig. 12, in which the dark gray lines correspond to the interface (cohesive) elements that were inserted to model the fracturing process. Only cohesive forces that relax the stresses of the adjacent elements are generated on these elements. When one of these interface elements comes into contact with another interface element that contains fluid (blue lines), the fluid pressure begins to

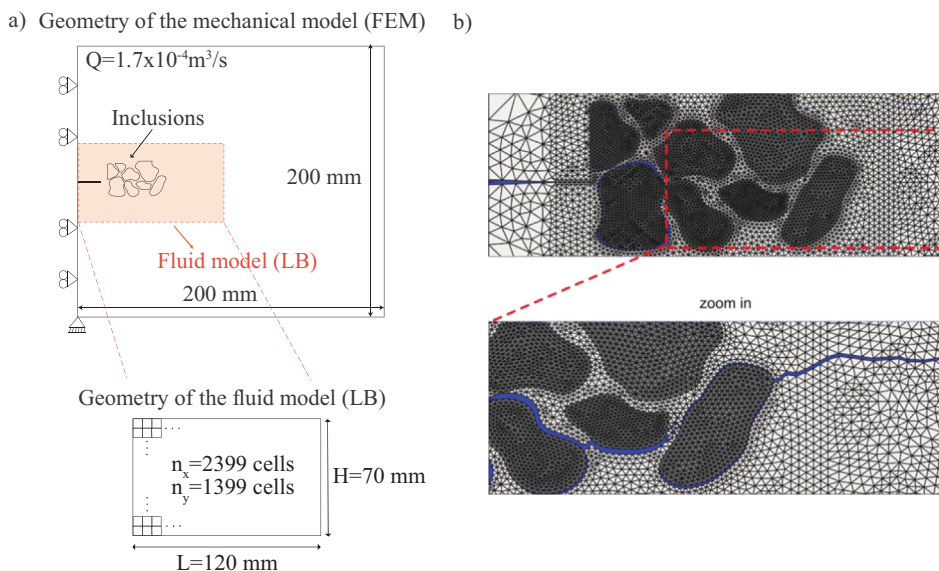


Fig. 11. a) Geometry and modeling boundary conditions of the hydraulic fracturing process in a medium with rigid inclusions; b) FEM mesh showing the hydraulic fracturing in a medium with rigid inclusions. The blue line represents the fluid surrounding the rigid inclusions (in dark gray).

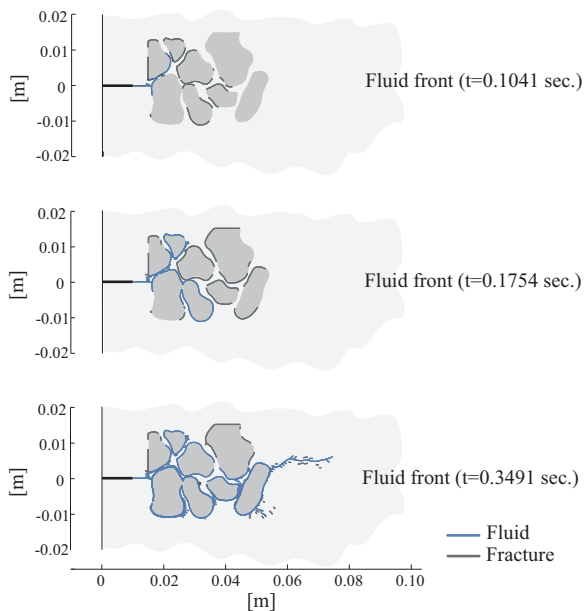


Fig. 12. Fracture growth in a medium with rigid inclusion. The black lines show the interface elements inserted into the finite element mesh. The blue lines shows the interface elements containing the injected fluid.

act inside the interface element and generates an opposite force to the cohesive forces. This accelerates the stress relaxation process for the adjacent elements and contributes to the fracture propagation. Because of the heterogeneity, not all of the interface elements that are inserted into the finite element mesh contain fluid.

#### 5.4. Comparison between numerical analysis of mixed Mode I-II hydraulic fracturing and laboratory test results

The model for a mixed rupture condition (Mode I-II) is validated by comparing the model results with laboratory test results. Based on Gonçalves et al.,<sup>66</sup> a hydraulic fracturing test of a granite sample was numerically simulated through the coupled numerical FEM-LB technique. Fig. 13a shows the geometry, the boundary conditions and the initial fracture locations through which the fluid is injected. A mapping

process is performed to generate a finite element mesh that represents the mineralogical distribution of the sample. Using a digital image of the sample, one defines the minerals by the colors of the pixels. The mapping process consists of associating the pixel locations with the elements of the finite element mesh so the color of the pixels in an element defines the type of material.

The laboratory test used a sample of Barre granite. However, no information on the mechanical and fracture properties of the minerals in this granite was available. The Stanstead and Barre granites have similar mechanical and fracture behaviors.<sup>67</sup> The mechanical and fracture properties of the Stanstead granite that are used in the numerical simulation are defined for each crystal mineral. For quartz, the Young's modulus and Poisson ratio of the material are  $E = 80.0$  GPa and  $\nu = 0.17$  respectively,  $\sigma_n = \sigma_t = 10.0$  MPa,  $\phi_n = \phi_t = 40$  N/m and  $\alpha = \beta = 2$ ; for feldspar, the Young's modulus and Poisson ratio of the material are  $E = 80.0$  GPa and  $\nu = 0.29$  respectively,  $\sigma_n = \sigma_t = 10.0$  MPa,  $\phi_n = \phi_t = 40$  N/m and  $\alpha = \beta = 2$ ; and for biotite, the Young's modulus and Poisson ratio of the material are  $E = 20.0$  GPa and  $\nu = 0.2$  respectively,  $\sigma_n = \sigma_t = 7.0$  MPa,  $\phi_n = \phi_t = 28$  N/m and  $\alpha = \beta = 2$ . The contacts between the minerals, which represent heterogeneity, have different fracture properties than those of the elements; for example, the contacts between quartz and feldspar have normal and shear cohesive strengths and a fracture energy of  $\sigma_n = \sigma_t = 8$  MPa and  $\phi_n = \phi_t = 32$  N/m, respectively. The values for the contacts between biotite and any other mineral are  $\sigma_n = \sigma_t = 6$  MPa and  $\phi_n = \phi_t = 24$  N/m. These parameters were adapted from Goodman<sup>68</sup> and Mahabadi.<sup>67</sup> As shown in Figure 23, the LB mesh is located in the central region of the finite element mesh to capture the fracture propagation. The fluid is injected into these fractures with a constantly increasing pressure, similarly to the laboratory test developed by Gonçalves et al.<sup>66</sup>

Figs. 13b and 14 present the sample and the simulation results. Both cases show good approximations of the fracture propagation paths and the type of coalescence formed in the rock between the two initial cracks. Fig. 14 compares the results for the sample tested in the laboratory and the finite element mesh at the end of the numerical simulation as well as the results of the previously described mineralogical mapping. The fracture propagation path depends on the mechanical properties of the materials. In both the sample and in the simulation, the fractures preferentially propagate through the contacts between two different minerals or through the biotite (which has a lower fracture

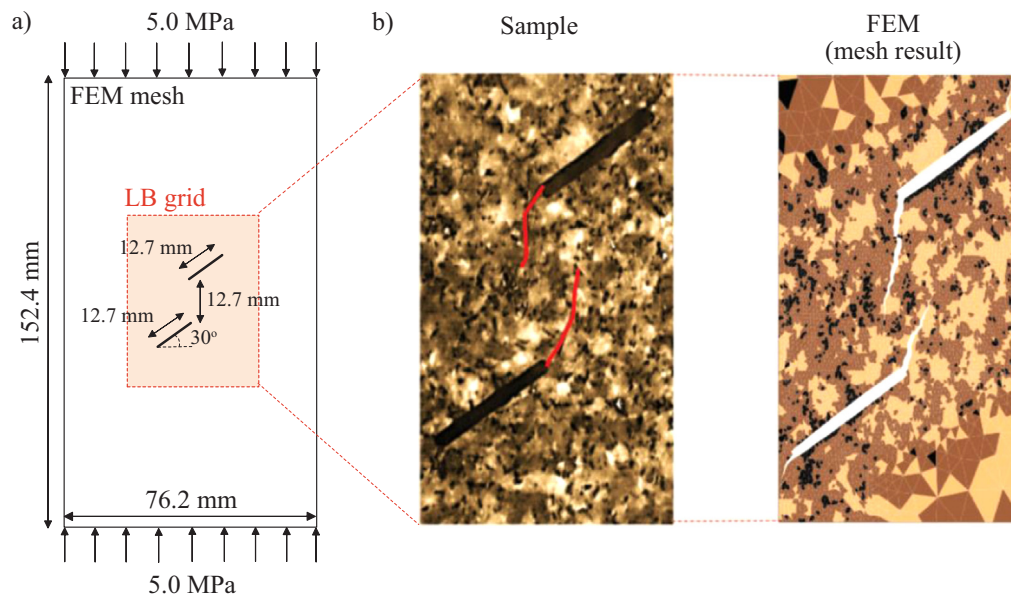


**Fig. 13.** a) Geometry and modeling boundary conditions to the hydraulic fracturing in the granite rock sample (Gonçalves et al.<sup>66</sup>). The LB mesh is located in the model center to capture fractures propagation; b) Comparison results between laboratory test (Gonçalves et al.<sup>66</sup>) and FEM-LB numerical modeling.

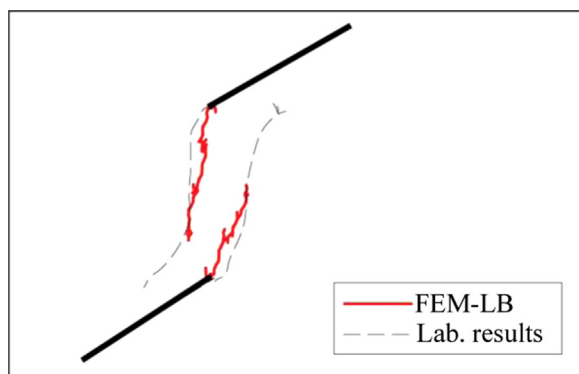


**Fig. 14.** Overlaid fracture propagation trajectories of laboratory test (Gonçalves et al.<sup>66</sup>) and coupled FEM-LB numerical simulation.

strength) than through the quartz or feldspar. To achieve a good approximation of the paths, the mineralogical distribution of the sample must be precisely represented in the finite element mesh, which requires a high quality digital image (Fig. 13b). The superposition of the paths that were obtained in the laboratory and those obtained from the numerical simulation show that they are similar (Fig. 14). Nonetheless, there are several small differences that are mainly due to the image quality used in the mineralogical mapping of the sample and/or the element size of the finite element mesh. The differences can also be due to the choice of fracture properties for the different material and interfaces. Although the modeling produces acceptable results, they are not completely identical to those of the physical tests. However, the coalescence type is the same in both cases, which demonstrates the capability of the coupled numerical method.

## 6. Conclusions

This study presents a method to couple the FEM and LB models. The extrinsic implementation of the PPR potential-based cohesive zone model is used to simulate the crack propagation. For the extrinsic implementation of the PPR model, interface elements are adaptively inserted into the finite element mesh to capture the fracturing process, which allows irregular fracture propagation paths. The LB model is used to simulate the fluid flow inside the fracture. The coupled FEM-LB

model simulates the hydraulic fracturing process by taking advantage of the ability of the LB model to simulate fluid flow through complex geometric shapes, such as fractures.

The use of interface (cohesive) elements allows the modeling of hydraulic fracture propagation. The fracture is formed between the mesh elements by duplicating the nodes (inter-element implementation). Therefore, the fracture properties are associated with the mesh facets (element faces that are shared with another element), which allows different values to be assigned, such as in heterogeneous materials or geological material with preexisting discontinuities.

The computational modeling scheme presented provided good results for hydraulic fracturing in geological materials. For the case considering preexisting discontinuities, the FEM-LB numerical coupling is able to describe their influence in the fracture propagation path. These results show that, depending on the discontinuity strength, the fracture propagation path could either bypass or cross a preexisting discontinuity. For the modeling of a material containing rigid inclusions, the fracture propagates surrounding the inclusions due to their higher fracture strength. Moreover, the contacts between these inclusions and the matrix material display a low rupture strength because the two materials have different mechanical properties, which forms a preferential path for fracture propagation. Numerical results for a rock material (granite) were consistent with the laboratory results and showed the same type of coalescence with few deviations in the propagation path. Nonetheless, these results could be improved, e.g. by incorporating mechanical and fracture properties that are more similar to those of the actual minerals in the rock, and by using a higher quality digital image for the mineral mapping, and/or a finite element mesh with element sizes that are similar to the digital image. However, the proposed coupled numerical FEM-LB technique can realistically model the hydraulic fracturing process in geomaterials.

The proposed methodology can be used in complex geological environment such as karst. In this case, the fluid injected to create a hydraulic fracture can flow into pre existing fractures (where the fluid flow follows Poiseuille type flow) and openings/caverns (where the fluid flow obeys Navier-Stokes equations). This complex condition can be solved by the LB model, but may not be easily approached by other numerical models developed to simulate hydraulic fracturing processes. The numerical scheme proposed in this work (FEM-LB) can be adapted for parallel computing and extended to 3D models – these are topics for

future research.

## Acknowledgements

The authors acknowledge "Coordenação de Aperfeiçoamento de Pessoal de Nível Superior" (CAPES) Foundation of the Ministry of Education of Brazil for the financial support for this research (Proc. 12144/13-4), and the endowment provided by the Raymond Allen Jones Chair at the Georgia Institute of Technology. In addition, we would like to thank Rodrigo Espinha for sharing the Tops library; Daniel Spring, from University of Illinois at Urbana-Champaign (UIUC), for the support on the PPR model implementation; Bruno Gonçalves, from the Massachusetts Institute of Technology (MIT), for the experimental test information; Omid Mahabadi, from Geomechanica Inc., for the useful discussions; and Oliver Giraldo-Londoño for helpful comments on the work and for his invaluable input to the manuscript. The information provided in this paper is the sole opinion of the authors and does not necessarily reflect the views of the sponsoring agencies.

## References

- Velloso R. *Numerical Analysis of Fluid Mechanical Coupling in Porous Media Using the Discrete Element Method [Ph.D. thesis] (In portuguese)*. Rio de Janeiro: Pontifical Catholic University of Rio de Janeiro; 2010.
- Eker E, Akin S. Lattice-Boltzmann simulation of fluid flow in synthetic fractures. *Transp Porous Media*. 2006;65:363–384.
- Barenblatt G. The formation of equilibrium cracks during brittle fracture: general ideas and hypothesis, axially symmetric cracks. *Appl Math Mech*. 1959;23:622–636.
- Barenblatt G. The mathematical theory of equilibrium cracks in brittle fracture. *Adv Appl Mech*. 1962;7:55–125.
- Dugdale D. Yielding of steel sheets containing cracks. *J Mech Phys Solids*. 1960;8:100–104.
- Hillerborg A, Modéer M, Petersson P. Analysis of crack formation and crack growth in concrete by means of fracture mechanics and finite elements. *Cem Concr Res*. 1976;6:773–782.
- Park K, Paulino GH. Cohesive zone models: a critical review of traction-separations relationships across fracture surfaces. *Appl Mech Rev, ASME*. 2011;64:0608021–06080220.
- Park K, Paulino GH, Roesler J. A unified potential-based cohesive model of mixed-mode fracture. *J Mech Phys Solid*. 2009;57:891–908.
- Spring D. *Failure Processes in Soft and Quasi-brittle Materials with Nonhomogeneous Microstructures [Ph.D. thesis]*. Urbana-Champaign: University of Illinois at Urbana-Champaign; 2015.
- Lecampion B. An extended finite element method for hydraulic fracture problems. *Commun Numer Methods Eng*. 2009;25:121–133.
- Taleghani D. Modeling simultaneous growth of multi-branch hydraulic fractures. In: *Proceedings of the 45th US Rock Mechanics/Geomechanics Symposium*. San Francisco; 2011.
- Chen Z. An abaqus implementation of the xfem for hydraulic fracture problems. In: *Proceedings of ISRM International Conference for Effective and Sustainable Hydraulic Fracturing*. Brisbane; 2013.
- Weber Y, Siebert P, Willbrand K, et al. The XFEM with an explicit-implicit crack description for hydraulic fracture problems. In: *Proceedings of the ISRM International Conference for Effective and Sustainable Hydraulic Fracturing*. Brisbane; 2013.
- Silvestre J, Vargas E, Vaz L, Soares A. Modelling of coupled fluid-mechanical problems in fractured geological media using enriched finite elements. *Int J Numer Anal Methods Geomech*. 2015;39:1104–1140.
- Bendezu M, Carvalho E, Roehl D, et al. Finite element modeling of the hydraulic fracture problem in impermeable media using a cohesive zone model. In: *Proceedings of the XXXIV Iberian-Latin American Congress on Computational Methods in Engineering – CILAMCE*; Pirenópolis; 2013.
- Frydman M, da Fontoura S. Numerical modeling of borehole pressurization. *Int J Rock Mech Min Sci*. 1997;34 [82.e1–e82.e14].
- Chen Z, Bunger A, Zhang X, et al. Cohesive zone finite element based modeling of hydraulic fractures. *Acta Mech Solid Sin*. 2009;22:443–452.
- Salehi S, Nygaard R. Finite-element analysis of deliberately increasing the wellbore fracture gradient. In: *Proceedings of the 44th US Rock Mechanics/Geomechanics Symposium*. Salt Lake City; 2010.
- Carrier B, Granet S. Numerical modeling of hydraulic fracture problem in permeable medium using cohesive zone model. *Eng Fract Mech*. 2012;79:312–328.
- Yao Y. Linear elastic and cohesive fracture analysis to model hydraulic fracture in brittle and ductile rocks. *Rock Mech Rock Eng*. 2012;45:375–387.
- Haddad M, Sepehrnoori K. Simulation of multiple-stage fracturing in quasi-brittle shale formation using pore pressure cohesive zone model. In: *Proceedings of the Unconventional Resources Technology Conference*. Denver; 2014.
- Hunsweek M, Shen Y, Lew A. A finite element approach to the simulation of hydraulic fractures with lag. *Int J Numer Anal Methods Geomech*. 2013;39:993–1015.
- Salimzadeh S, Paluszny A, Zimmerman RW. Three-dimensional poroelastic effects during hydraulic fracturing in permeable rocks. *Int J Solids Struct*. 2017;108:153–163.
- Torres S, Castaño J. Simulation of the hydraulic fracture process in two dimensions using a discrete element method. *Phys Rev*. 2007;75:066109–1 – 066109-9.
- Choi S. Interpretation of shut-in pressure in hydrofracturing pressure-time records using numerical modeling. *Int J Rock Mech Min Sci*. 2012;50:29–37.
- Galindo-Torres S, Behrafar S, Scheuermann A. A micromechanical model for studies of hydraulic fracturing. *Comput Methods Recent Adv Geomech*. 2015;255:1575–1580.
- Mejía Camones L, Vargas E, de Figueiredo R, et al. Application of the discrete element method for modeling of rock crack propagation and coalescence in step-path failure mechanism. *Eng Geol*. 2013;153:80–94.
- Mahabadi O, Lisjak A, Munjiza A, et al. Y-Geo: a new combined finite-discrete element numerical code for geomechanical applications. *Int J Geomech*. 2012;12:676–688.
- Lisjak A, Grasselli G, Vietor T. Continuum-discontinuum analysis of failure mechanisms around unsupported circular excavations in anisotropic clay shales. *Int J Rock Mech Min Sci*. 2013;65:96–115.
- Lisjak A, Grasselli G. A review of discrete modeling techniques for processes in discontinuous rock masses. *Int J Rock Mech Geotech Eng*. 2014;6:301–314.
- Lisjak A, Mahabadi O, Kaifosh P, et al. A preliminary evaluation of an enhanced FDEM code as a tool to simulate hydraulic fracturing in foamed rock masses. In: *Proceedings of the EUROCK 2014 – Rock Engineering and Rock Mechanics: Structures in and on Rock Masses*. Vigo; 2014.
- Yan CZ, Zheng H, Sun GH, et al. Combined finite-discrete element method for simulation of hydraulic fracturing. *Rock Mech Rock Eng*. 2016;49(4):1389–1410.
- Yan CZ, Zheng H. A two-dimensional coupled hydro-mechanical finite-discrete model considering porous media flow for simulating hydraulic fracturing. *Int J Rock Mech Min Sci*. 2016;88:115–128.
- Yan CZ, Zheng H. FDEM-flow 3D: a 3D hydro-mechanical coupled model considering the pore seepage of a rock matrix for simulating three-dimensional hydraulic fracturing. *Comput Geotech*. 2017;81:212–228.
- Yan CZ, Jiao YY. A 2D fully coupled hydro-mechanical finite-discrete element model with real pore seepage for simulating the deformation and fracture of porous medium driven by fluid. *Comput Struct*. 2018;196:311–326.
- Yan CZ, Jiao YY. A fully coupled three-dimensional hydro-mechanical finite discrete element approach with real porous seepage for simulating 3D hydraulic fracturing. *Comput Geotech*. 2018;96:73–89.
- Falk M, Needleman A, Rice A. A critical evaluation of cohesive zone models of dynamic fracture. *J Phys*. 2001;11(5):43–50.
- Blal N, Daridon L, Monerie Y, Pagano S. Artificial compliance inherent to the intrinsic cohesive zone models: criteria and application to planar meshes. *Int J Fract*. 2012;178:71–83.
- Leon S. *Adaptive Finite Element of Fracture: From Plastic Deformation to Crack Propagation [Ph.D. thesis]*. Urbana-Champaign: University of Illinois at Urbana-Champaign; 2015.
- de Figueiredo R. *Application of the Dynamic Relaxation Technic in the Solution of Geotechnical Problems [M.Sc. Dissertation] (In Portuguese)*. Rio de Janeiro: Pontifical Catholic University of Rio de Janeiro; 1991.
- Felippa CA. *Introduction to Finite Element Methods (ASEN 5007)*. (<https://www.colorado.edu/engineering/CAS/courses/d/IFEM/d/>).
- Bathe KJ. *Finite Elements Procedures in Engineering Analysis*. New Jersey: Prentice-Hall; 1982.
- Smith GP. *Numerical Solution of Partial Differential Equations: Finite Difference Methods*. 3rd ed. Great Britain: Clarendon Press; 1986.
- Zhang Z. *Extrinsic Cohesive Modeling of Dynamic Fracture and Microbranching Instability Using a Topological Data Structure [Ph.D. thesis]*. Urbana-Champaign: University of Illinois at Urbana-Champaign; 2007.
- Espinha R, Celes W, Rodrigues N, et al. Partops: compact topological framework for parallel fragmentation simulations. *Eng Comput*. 2009;25:345–365.
- Paulino G, Celes W, Espinha R, et al. A general topology-based framework for adaptive insertion of cohesive elements in finite element meshes. *Eng Comput*. 2008;24:59–78.
- Park K, Paulino GH. Computational implementation of the PPR potential-based cohesive model in ABAQUS: educational perspective. *Eng Fract Mech*. 2012;93:239–262.
- Mohamad A. *Lattice-Boltzmann Method – Fundamentals and Engineering Applications with Computer Codes*. London: Springer; 2011.
- Salinas S. *Introduction to Statistical Physics*. Berlin: Springer; 2001.
- Bhatnagar P, Gross E, Krook M. A model for collision process in gases. I. Small amplitude processes in charged and neutral one-component system. *Phys Rev*. 1953;94:511–525.
- Golbert D. *Modelos de lattice-Boltzmann aplicados à simulação computacional do escoamento de fluidos incompressíveis [M.Sc. dissertation] (In Portuguese)*. Petropolis: National Laboratory of Scientific Computation-LNCC; 2009.
- Gladrow W. *Lattice-Gas Cellular Automata and Lattice Boltzmann Models – An Introduction*. Berlin: Springer; 2000.
- He X, Luo L. Lattice-Boltzmann model for the incompressible Navier-Stokes equation. *J Stat Phys*. 1997;88:927–944.
- Guiet J, Reggio M, Teyssedou A. Implementation and application of the lattice-Boltzmann method using MatLab. *Eng Appl Comput Fluid Mech*. 2011;5:117–126.
- Shi Y, Zhao T, Guo Z. Lattice-Boltzmann method for incompressible flows with large pressure gradients. *Phys Rev*. 2006;73 [026704-1 to 026704-11].
- Lin Z, Fang H, Tao R. Improved lattice-Boltzmann model for incompressible two-dimensional steady flows. *Phys Rev*. 1996;54:6323–6330.
- Noble D, Torczynski J. A lattice-Boltzmann method for partially saturated computational cells. *Int J Mod Phys*. 1998;9:1189–1201.
- Barber RW, Emerson DR. The influence of Knudsen number on the hydrodynamics

- development length within parallel plate micro-channels. *Adv Fluid Mech IV*. 2012;36:207–216.
59. Dan C, Srivastava S, Harting J, et al. Lattice-Boltzmann simulations of fluid flows at the finite Knudsen number. In: *Proceedings of the Conference on Modelling Fluid Flow (CMFF'12). The 15th International Conference of Fluid Flow Technologies*. Budapest; 2012.
60. Detournay E. Propagation regimes of fluid-driven fractures in impermeable rocks. *Int J Geomech*. 2004;4:35–45.
61. Garagash DI. Propagation of plane-strain hydraulic fracture with a fluid lag: early-time solution. *Int J Solids Struct*. 2006;43:5811–5835.
62. Sukop MC, Thorne DT. *Lattice Boltzmann Modeling: An Introduction for Geoscientists and Engineers*. Berlin: Springer; 2006.
63. Bahorich B, Olson J. Examining the effect of cemented natural fractures on hydraulic fracture propagation in hydrostone block experiments. In: *Proceedings of the SPE Annual Technical Conference and Exhibition*. San Antonio; 2012.
64. Fu P, Cruz L, Moos D., et al. Numerical investigation of a hydraulic fracture bypassing a natural fracture in 3D. In: *Proceedings of the 49th US Rock mechanics/Geomechanics Symposium*. San Francisco; 2015.
65. Blanton T. An experimental study of interaction between hydraulically induced and preexisting fractures. In: *Proceedings of the SPE Unconventional Gas Recovery System*. Pittsburgh; 1982: 559–571.
66. Gonçalves da Silva B, Li B, Moradian Z, et al. Development of a test setup capable of producing hydraulic fracturing in the laboratory with image and acoustic emission monitoring. In: *Proceedings of the 49th US Rock Mechanics/Geomechanics Symposium*. San Francisco; 2015.
67. Mahabadi O. *Investigating the Influence of Micro-scale Heterogeneity and Microstructure on the Failure and Mechanical Behavior of Heomaterials [Ph.D. thesis]*. Toronto: University of Toronto; 2012.
68. Goodman RE. *Introduction to Rock Mechanics*. 2nd ed. New York: Wiley; 1989.